Microphase Separation in Model 3-Miktoarm$^+$ Star Copolymers (Simple Graft) and Terpolymers. 1. Statics and Kinetics

G. Floudas*

Foundation for Research and Technology (FORTH)–HELLAS, Institute of Electronic Structure and Laser, P.O. Box 1527, Heraklion 711 10 Crete, Greece

N. Hadjichristidis‡ and H. Iatrou‡

Department of Chemistry, University of Athens, Panepistimiopolis, Zografou 157 71, Athens, Greece

T. Pakula and E. W. Fischer

Max-Planck-Institut für Polymerforschung, Postfach 3148, D-55021 Mainz, FRG

Received July 20, 1994; Revised Manuscript Received September 7, 1994®

ABSTRACT: The static and kinetic aspects of the order–disorder transition (ODT) in newly synthesized model 3-miktoarm star copolymer (simple graft) of SI2 type, (polystyrene)(polyisoprene)$_2$, and a 3-miktoarm star terpolymer of SIB type, (polystyrene)(polyisoprene)(polybutadiene), have been studied using small-angle X-ray scattering (SAXS) and rheology. The morphology and the order–disorder transition temperature (T_{ODT}) have been identified from the two-dimensional SAXS patterns with shear-oriented samples. Hexagonally ordered cylindrical microdomains aligned along the direction of shear and with T_{ODT} = 379 K have been formed for both samples studied. The SAXS profiles at temperatures well above the T_{ODT} have been fitted to the mean-field theory (MFT) for graft copolymers. Near the ODT deviations from the theory have been observed and the SAXS data provide unambiguous evidence for the existence of fluctuations. The T_{ODT} obtained from rheology is in excellent agreement with the one from SAXS. Discontinuities in the SAXS peak intensity and in the storage modulus near the T_{ODT} are more pronounced in these systems as compared to linear diblocks. The ordering kinetics have been studied with rheology and complementary with SAXS. The width of the kinetically accessible metastable region is enlarged as compared to linear diblocks. For shallow quenches the ordering proceeds by heterogeneous nucleation and growth of three-dimensional grains with cylindrical microstructure. Our kinetic studies probe the metastable states near but below the T_{ODT}.

Introduction

Block copolymers are important commercial materials with a great scientific interest because they can undergo a microphase separation from a homogeneous (disordered) phase to a variety of spatially periodic (ordered) phases.[1] The temperature where this occurs is called the microphase separation temperature (T_{MST}) or the order–disorder temperature (T_{ODT}). Chemically joining two homopolymers to form a diblock copolymer increases the compatibility, and this is reflected in the reduction of the critical temperature for phase separation as compared to a homopolymer blend. Compatibility can be further increased by changing the molecular architecture. For this purpose, triblock, star, and recently graft and miktoarm copolymers have been made and in general:

$$(\chi N)_{c,blend} < (\chi N)_{ODT,diblock} < (\chi N)_{ODT,graft} < (\chi N)_{ODT,triblock} < (\chi N)_{ODT,star} \quad (1)$$

where χN is the product of the interaction parameter χ with the number of segments N and $(\chi N)_{c\ or\ ODT}$ is the critical value of χN for stability of the disordered state. Given that, in the simplest approximation, χ is inversely proportional to temperature, inequality (1) means that a melt of triblock or graft copolymers will remain in the homogeneous (disordered) phase for low temperatures where a melt of linear diblocks is already microphase separated.

The first theory which describes the phase behavior of linear diblock melts in the weak segregation limit was formulated by Leibler.[2] In this mean-field theory (MFT) the structure factor in the disordered phase is

$$\frac{N}{S_L(Q)} = F(x,f) - 2\chi N \quad (2)$$

where $F(x,f)$ is a combination of certain Debye functions, $x = Q^2R_G^2$ ($Q = (4\pi/\lambda)\sin(\theta/2)$ is the scattering wavevector, λ = 0.154 nm is the wavelength of X-rays, and θ is the scattering angle), and f is the composition ($=N_A/N$). For symmetric diblocks ($f = 1/2$) the MFT predicts a second-order transition to the lamellar phase for a critical value of $(\chi N)_c = 10.5$. The ODT is predicted to be first order at $f \neq 0.5$ and is identified as a transition to a body-centered cubic (bcc) structure. Fredrickson and Helfand[3] introduced fluctuation corrections which were found to be on the order of $\bar{N}^{-1/3}$, where $\bar{N}$ is the Ginzburg parameter ($=Na^6/u^2$, where a and u are the statistical segmental length and volume, respectively). The spinodal was completely suppressed, and the transition for $f = 1/2$ was a weak, first-order transition at:

$$\chi N_{ODT} = 10.5 + 41\bar{N}^{-1/3} \quad (3)$$

The effects of fluctuations have been studied experimentally by small-angle neutron scattering (SANS), small-angle X-ray scattering (SAXS), and rheology mainly on the systems poly(ethylenepropylene-*b*-ethylethylene) (PEP–PEE)[4–7] and poly(styrene-*b*-isoprene) (SI).[8–10] Since then, the mean-field theory has been generalized for triblock,[11] graft, and star[12] copolymers

$^+$ From the Greek word *μικτός* meaning mixed.
‡ Also at FORTH.
® Abstract published in *Advance ACS Abstracts,* November 1, 1994.

0024-9297/94/2227-7735$04.50/0

by Olvera de la Cruz, Sanchez, and Mayes and for asymmetric[13] and symmetric[14] comb copolymers. Fluctuation corrections have also been incorporated for triblock[15] and star copolymers.[16]

In this paper, we study the static and kinetic aspects near the ODT for two new polymer architectures: a 3-miktoarm star copolymer (simple graft) of SI2 type, (polystyrene)(polyisoprene)$_2$, and a 3-miktoarm star terpolymer of SIB type, (polystyrene)(polyisoprene)-(polybutadiene). The synthesis[17] and morphology[18] of such copolymers have been reported only recently, and this is the first experimental work on the statics and kinetics near the ODT. We employ SAXS and rheology for temperatures below and above the ODT. We analyze the SAXS profiles using the MFT for graft copolymers. We find good agreement at temperatures $T \gg T_{ODT}$. However, our SAXS results provide unambiguous evidence for fluctuation effects as we approach the transition. The ordering kinetics have also been studied by rheology and SAXS by making quench experiments from the disordered to the ordered state and by monitoring the temporal evolution of G^* and $I(Q)$, where G^* is the complex shear modulus and $I(Q)$ is the SAXS peak intensity. We find that the ordering process is reminiscent of the crystallization isotherms of semicrystalline materials but the width of the kinetically accessible metastable region is very different from linear diblocks. This makes the observation of metastable states with rheology and SAXS in miktoarm copolymers and terpolymers easier.

Experimental Section

Synthesis and Characterization. The synthesis of the 3-miktoarm star copolymer SI2 (also called simple graft) will be given in detail in a forthcoming paper.[19] The basic reactions used are schematically the following:

$$\mathrm{PSLi} + \text{excess } \mathrm{CH_3SiCl_3} \rightarrow \mathrm{CH_3Si(PS)Cl_2} + \mathrm{LiCl} + \mathrm{CH_3SiCl_3}\uparrow$$

$$\mathrm{CH_3Si(PS)Cl_2} + \text{excess PILi} \rightarrow \mathrm{CH_3Si(PS)(PI)_2} \qquad \text{(SI2)}$$

For the synthesis of the 3-miktoarm star terpolymer SIB the procedure published elsewhere[17] was followed. A schematic representation of the sequence of reactions used is shown below:

$$\mathrm{PILi} + \text{excess } \mathrm{CH_3SiCl_3} \rightarrow \mathrm{CH_3Si(PI)Cl_2} + \mathrm{LiCl} + \mathrm{CH_3SiCl_3}\uparrow$$

$$\mathrm{CH_3Si(PI)Cl_2} + \mathrm{PSLi}^{\text{titration}} \rightarrow \mathrm{CH_3Si(PI)(PS)Cl} + \mathrm{LiCl}$$

$$\mathrm{CH_3Si(PI)(PS)Cl} + \text{excess PBdLi} \rightarrow \mathrm{CH_3Si(PS)(PI)(PBd)} \qquad \text{(SIB)}$$

where PI is polyisoprene, PS polystyrene, and PBd polybutadiene. The purification procedures for monomer, the linking agent CH_3SiCl_3, and the solvent benzene to the standards required for anionic polymerization have been described in detail elsewhere.[20] *sec*-BuLi, prepared in vacuo from *sec*-butyl chloride and a lithium dispersion in hexane, was used as the initiator for all polymerizations. All manipulations were performed in evacuated n-BuLi-washed and benzene-rinsed glass reactors provided with break-seals and constrictions. The unlinked excess of the linear PBd or PI was eliminated by fractionation which was carried out by adding methanol to the miktoarm star solution (~1% w/w).

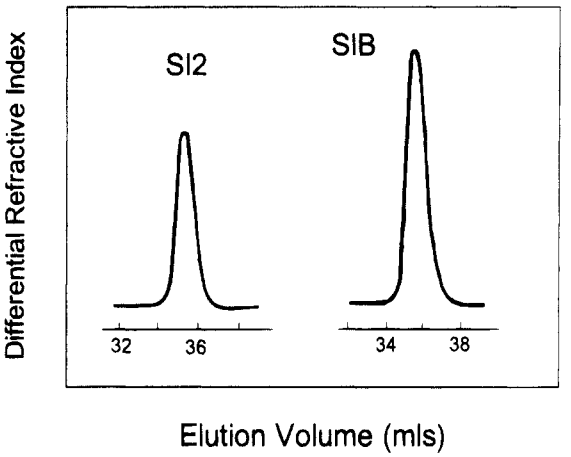

Figure 1. SEC chromatograms of the 3-miktoarm star (graft) copolymer SI2 and terpolymer SIB in THF at 298 K.

The determinations of the polydispersity index ($\bar{M}_w/\bar{M}_n$), the weight-average molecular weight ($\bar{M}_w$), and the number-average molecular weight ($\bar{M}_n$) were carried out by size-exclusion chromatography (SEC; Waters Model 510 pump, 401 differential refractometer, four μ-Styragel columns 10^3-10^6 Å, THF, 303 K), low-angle laser light scattering (chromatix KMX-6, $\lambda = 633$ nm, THF, 298 K), differential laser refractometry (chromatix KMX-16, $\lambda = 633$ nm, THF, 298 K), membrane osmometry (Wescan Model 230, toluene, 310 K), and vapor pressure osmometry (Wescan Model 233, toluene, 323 K). The dienic precursors, PI and PBd, analyzed by ^{1}H- and ^{13}C-NMR (Bruker AC200) spectroscopy in $CDCl_3$ at 303 K were found to have typical microstructures.[17] The polystyrene content was obtained from the ^{1}H-NMR spectra and by UV analysis at 269 and 262 nm. The SEC chromatograms of SI2 and SIB are given in Figure 1, and the characteristics of the precursors and the fractionated miktoarm stars are given in Table 1.

Two glass transition temperatures have been identified by differential scanning calorimetry (DSC). Samples were first cooled to 125 K at a rate of 20 K/min and subsequently heated to 403 K at 10 K/min. This procedure was repeated for a second heat, but only in the first heat were two T_g's clearly resolved with low and high values corresponding to the isoprene- and styrene-rich phases, respectively. The two T_g's were 217 and 335 K for SI2 and 204 and 338 K for SIB.

Small-Angle X-ray Scattering (SAXS). The SAXS measurements were made with a Kratky compact camera (Anton Paar KG) equipped with a one-dimensional position-sensitive detector (M. Braun). The Ni-filtered Cu Kα radiation (λ = 0.154 nm) was used from a Siemens generator (Kristalloflex 710 H) operating at 35 kV and 30 mA. The sample was kept in the camera under vacuum in a special furnace, and the temperature was maintained by means of a temperature controller. Measurements 1 h long were made at intervals of 3 K within the range 298–423 K, with a stability better than ±0.2 K. Changes between successive temperatures were completed within ~5 min, and a 30 min waiting time was preset for equilibration . The smeared intensity data were collected in a multichannel analyzer and transferred to a VAX computer for further analysis. Smeared intensities were subsequently corrected for absorption, background scattering, and slit-length smearing. Primary beam intensities were determined, in absolute units, by using the moving slit method.

For the investigation of the morphology, a different SAXS setup was used with a 18-kW rotating-anode X-ray source (Rigaku) with a pinhole collimation and a two-dimensional detector (Nicolet) with 512 × 512 pixels. The Ni-filtered Cu Kα radiation was used, and three collimators prior to the sample resulted in a beam diameter of ~1 mm. The sample-to-detector distance was 1.21 m. Two orientations were used: (i) edge and (ii) through view.

Rheology. The storage and loss moduli G' and G'' have been measured with a Rheometrics RMS 800 in the oscillatory mode and with a parallel-plate sample geometry. The sample

Table 1. Characteristics of the 3-Miktoarm Star (Graft) Copolymer SI2 and Terpolymer SIB

sample	$\bar{M}_n \times 10^{-3}$ [a] (PS) precursor	$\bar{M}_n \times 10^{-3}$ [a] (PI) precursor	$\bar{M}_n \times 10^{-3}$ [a] (PBd) precursor	$\bar{M}_n \times 10^{-3}$ [b] (star)	$\bar{M}_w \times 10^{-3}$ [c] (star)	$\bar{M}_w/\bar{M}_n$ [d] star	PS content (% w/w) (star) UV	NMR	$\bar{M}_n$ [e]
SI2	7.6	8.0		23.7	25.5	1.03	33	32	32
SIB	7.9	8.2	7.7	23.8	24.7	1.04	33	34	33

[a] Vapor pressure osmometry in toluene at 323 K. [b] Membrane osmometry in toluene at 310 K. [c] Low-angle laser light scattering in THF at 298 K. [d] Size-exclusion chromatography in THF at 303 K. [e] Calculated from the $\bar{M}_n$ values of the precursors.

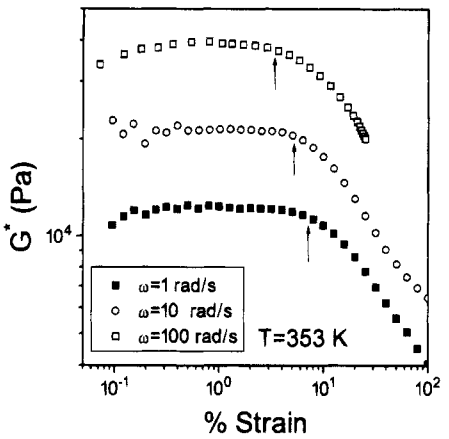

Figure 2. Strain dependence of the magnitude of the complex shear modulus G^* for the graft copolymer SI2, at 353 K at three frequencies, as indicated. Arrows separate the linear from the nonlinear viscoelastic range.

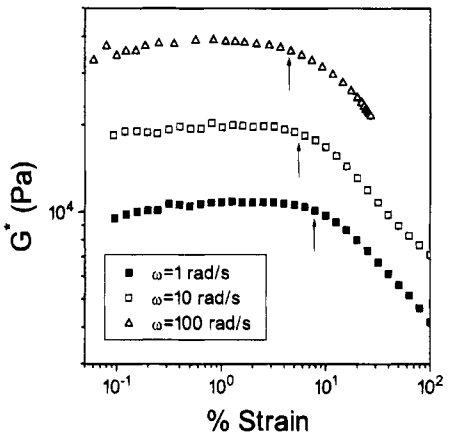

Figure 3. Strain dependence of the magnitude of the complex shear modulus for the 3-miktoarm star terpolymer SIB at 353 K at three frequencies as indicated.

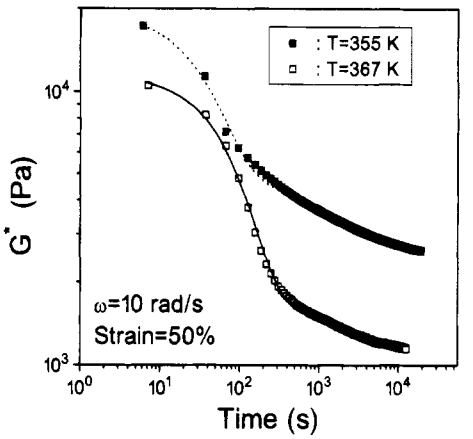

Figure 4. Magnitude of the complex shear modulus of SI2 during isochronal/isothermal time scans at two temperatures as indicated. The frequency is 10 rad/s and the strain amplitude 50%, which are values well within the nonlinear regime (see Figure 2). Lines are fits to eq 4 (see text).

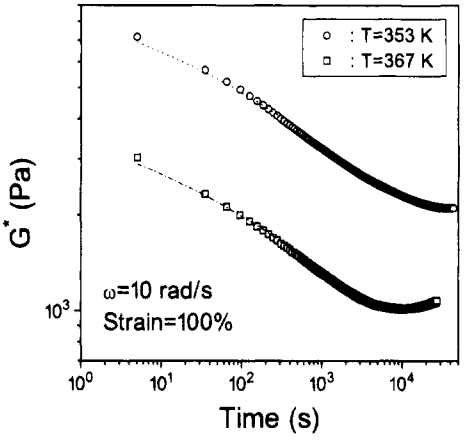

Figure 5. Magnitude of the complex shear modulus of SIB during isochronal/isothermal time scans at two temperatures as indicated. Shearing conditions are within the nonlinear regime (see Figure 3). Lines are fits to eq 4 (see text).

temperature was controlled between 298 and 398 K with a nitrogen gas. Four different experiments were made. In the first experiment we investigated the effect of the strain amplitude on the complex shear modulus, $G^* = (G'^2 + G''^2)^{1/2}$ for the two samples. The strain dependences of G^* for SI2 and SIB are shown in Figures 2 and 3, respectively, for strain amplitudes in the range 0.1−100% (only three frequencies are shown in Figures 2 and 3). Arrows separate the linear from the nonlinear viscoelastic range, and this separation clearly depends on frequency. On the basis of the different dynamic responses in the two regions, we have used strain amplitudes smaller than the critical ones (linear viscoelastic range) for the following experiments: (i) isochronal temperature scans (at $\omega = 0.5$ rad/s), (ii) isothermal frequency scans, and (iii) isochronal/isothermal time scans. In the fourth experiment we have used high enough strain amplitudes (within the nonlinear viscoelastic range) with the purpose to induce orientational order in the material. For this purpose we used a single frequency $\omega = 10$ rad/s and a strain amplitude of 50% (SI2) and 100% (SIB) for two temperatures, one at $T = 355$ K, which is near but above the styrene T_g, and a second at $T = 367$ K, which is near but below the T_{ODT} (=379 K). The time dependencies of G^* during continuous oscillatory shear at the two temperatures are shown in Figures 4 and 5 for SI2 and SIB, respectively.

In this type of experiment, G^* is a decreasing function of time and the magnitude of this decrease depends on the temperature and on the system. This decrease results from the elimination of interfaces perpendicular to the shear direction and reorientation of cylinder domains along the shear direction.[21] For SI2, oriented at 367 K, $G^*(t)$ decreased by 1 order of magnitude for a time interval of 10^4 s. Moreover, $G^*(t)$ in SI2 displayed a clear two-step decay as compared to a single decay in SIB. In the latter system, however (Figure 5), there is an upturn in $G^*(t)$ for $t > 10^4$ s which has not been seen in linear diblocks and may be associated with the structural changes occurring in the vicinity of 367 K (see below). The shapes of the recorded curves of G^* vs t depend on thermal history and therefore on the kinetics of morphological reorientation and on complex relationships between morphology and mechanical properties of the system. In order to extract the information about the kinetics of reorientation, such relationships should be known, for example, in the form of suitable mechanical models. Because of the lack of such

models relating the morphological orientation parameters with the macroscopic mechanical properties, we analyze the recorded dependencies directly by means of a sum of the well-known Kohlrausch–Williams–Watts (KWW) functions:

$$G^*(t) = \Sigma_i \Delta G_i^* \exp[-(t/\tau)^{\beta_i}] \quad (4)$$

where ΔG^*, τ, and β are amplitudes of the modulus relaxation, relaxation times, and shape parameters, respectively. For the graft SI2 (Figure 4) the modulus seems to relax in two steps and the fit of eq 4 revealed two processes: a "fast" one being of the Debye type ($\beta = 1$) and a "slow" very broad one with $\beta \approx 0.1$. The fast process of the modulus relaxation can be attributed to a domain reorientation toward the shear direction which occurs within ~100 s and the slow stretched exponential process to the perfection of the oriented morphology consisting, for example, in coalescence of grains into a monodomain. The distribution of relaxation times of the latter process is very broad as indicated by the low value of β (≈0.1). A 367 K the ratio of the amplitudes of the two processes ($\Delta G_1^*/\Delta G_2^*$) is 2.6, indicating that the modulus relaxation is accomplished in 72% via the fast process. For SIB the fast process is not observed and the slow process with a broad distribution of relaxation times ($\beta \approx 0.1$) controls the modulus relaxation (Figure 5).

Morphology. The shear-oriented samples were examined with a two-dimensional SAXS detector as a function of T. The first sample SI2 was oriented at 355 K at a frequency of 10 rad/s with a strain amplitude of 50%. The two-dimensional patterns taken with X-rays parallel (tangential view) and perpendicular (normal view) to the shear direction are shown in Figure 6 at four temperatures: $T = 298$, 358, 376, and 379 K. The patterns shown in Figure 6 are of hexagonal symmetry with cylinders aligned along the direction of shear.[22] The normal view is also shown at some temperatures and shows two Bragg reflections at Q higher than Q^*. In principle, a perfect orientation of cylinders with the 100 planes parallel to the shear plane should produce no scattering at Q^* but only reflections at $\pm(3Q^*)^{1/2}$. Notice that there exist some "isotropic" components at all temperatures which may arise from some residual misalignment of cylinders. A pertinent feature of Figure 6 is that the cylindrical morphology persists up to $T_{ODT} - T \approx 3$ K. At the ODT ($T_{ODT} = 379$ K) the scattering pattern turns into isotropic. When heating an asymmetric linear diblock copolymer, mean-field theory would predict the following sequence: hexagonal → bcc → isotropic. The absence of the intermediate bcc structure from the scattering patterns of asymmetric diblocks has been discussed in terms of fluctuation effects which become important near the transition.[23] This situation here (Figure 6) is reminiscent of the behavior in asymmetric, linear diblock copolymers.

Two SIB samples were oriented at 10 rad/s with a strain amplitude of 100% at 352.6 and 367.3 K. The temperature dependence of the two-dimensional pattern was studied for temperatures $T = 298$, 358, 376, and 379 K. In the temperature range $\Delta T = 298–375$ K, the structure was that of cylinders aligned along the direction of shear as with the SI2 sample. The sample disorders at $T = 379$ K, which is exactly the same ODT temperature as for the SI2 sample, but at 376 K ($T_{ODT} - T = 3$K) a different structure was observed, both from the tangential and normal views. This point, however, needs further investigation.

Results and Discussion

Small-Angle X-ray Scattering. Scattering of X-rays from a single-component system is caused by electron density fluctuations. Additionally, concentration fluctuations exist in a two-component system. The former are given by:

$$I_d = n^2 k_B T \beta_T \quad (5)$$

where n is the average electron density and β_T is the isothermal compressibility. The latter are given by:

$$I_c = \Delta n^2 V S_c(Q) \quad (6)$$

where Δn ($=n_A - n_B$) is the difference in the electron number densities of A and B (the scattering contrast), V is the volume of a chain, and $S_c(Q)$ is the static structure factor for concentration fluctuations. Evaluation of the scattering caused by concentration fluctuations requires the subtraction of the contribution from the pure density fluctuations. This is usually made by extrapolating the measured intensity from high Q to $Q = 0$ and assumes that the "background" intensity is caused solely by density fluctuations. Our earlier work[24,25] on SAXS from two-component systems has shown that the SAXS background contains density *and* concentration fluctuations. A safer method of accounting for the density fluctuations involves measuring the $\beta_T(T)$ and calculating I_d from eq 5. This intensity is then subtracted, at every temperature, from the measured SAXS profiles. Some typical SAXS data for the SI2 simple graft copolymer, corrected for the density fluctuations, are shown in Figure 7, for temperatures in the range $378 < T < 423$ K. There is a big discontinuity in the $I(Q^*)$ for temperatures between 378 and 381 K. From the two-dimensional patterns of Figure 6, the T_{ODT} was estimated at 379 K which is in a very good agreement with the estimation based on Figure 7. Solid lines in Figure 7 are fits to the MFT for graft copolymers.

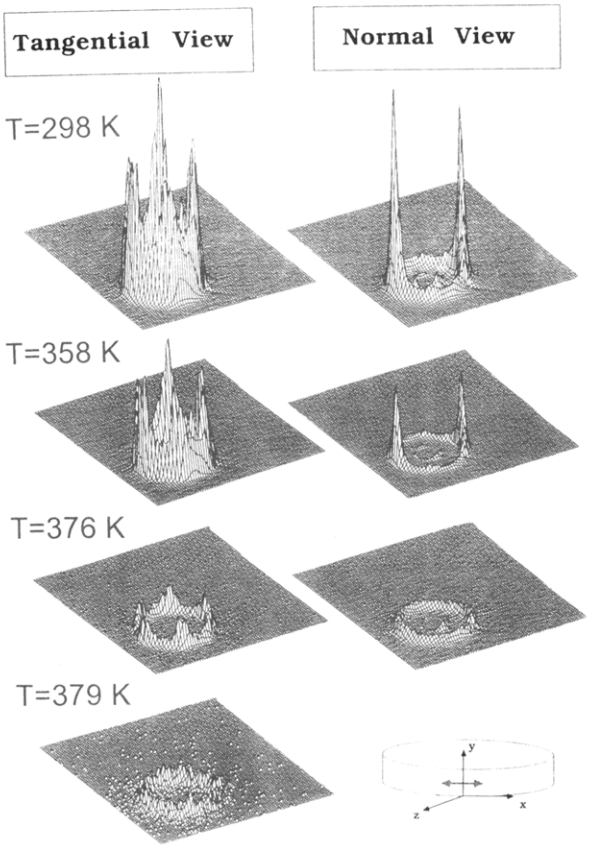

Figure 6. Representative SAXS patterns for the SI2 graft copolymer. The sample was oriented at $T = 355$ K with a strain amplitude of 50% at a frequency of 10 rad/s (Figure 4). The coordinate system used is shown on the lower corner: (x) tangential, (y) normal, and (z) radial directions. The tangential (left) and normal (right) views are shown. The data indicate a hexagonal structure with cylinders aligned along the direction of shear. The sample disorders at 379 K. The vertical axis has been scaled arbitrarily to make the patterns observable.

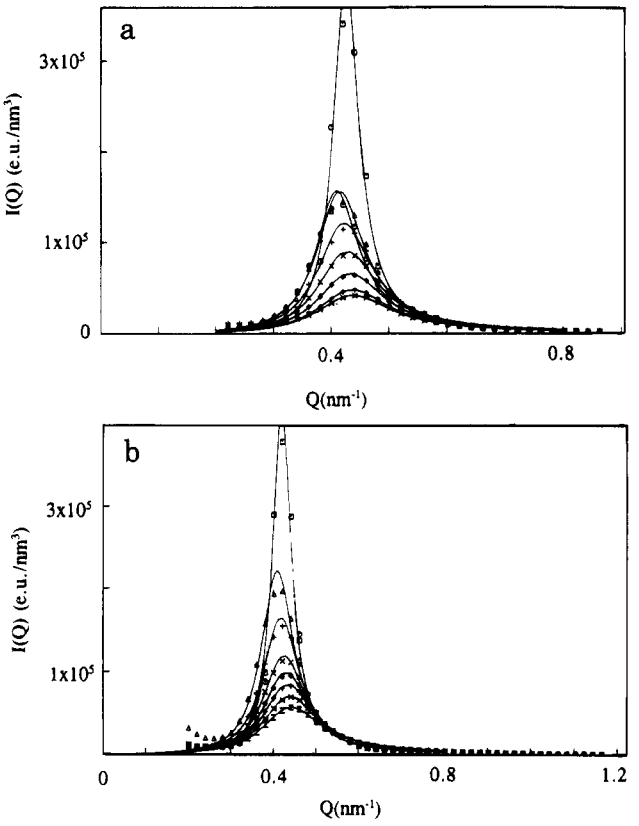

Figure 7. (a) SAXS profiles of SI2 at different temperatures: 378, 381, 391, 401, 408, 414, 420, and 423 K from top to bottom. (b) SAXS profiles of SIB at different temperatures: 373, 383, 393, 398, 408, 413, 418, and 423 K from top to bottom.

According to the MFT for the microphase separation of graft copolymers,[12] the phase behavior is defined by three variables: χN, f, and τ. The first is the product of the interaction parameter χ with the total degree of polymerization N. The second is the fraction of A monomers in the copolymer, and the third is the fractional position along the A chain backbone at which the B graft is chemically linked. The structure factor now depends on f *and* τ:

$$\frac{N}{S(Q)} = \frac{D(f,x) + D(1-f,x) + 2F_{\tau f}(x)\,F_{1-f}(x)}{D(f)\,D(1-f,x) - (F_{\tau f}(x)\,F_{1-f}(x))^2} - 2\chi N \tag{7}$$

where

$$D(f,x) = \frac{2}{\chi^2}(fx + e^{-fx} - 1), \qquad x = Q^2 R_G{}^2 \tag{8}$$

is the Debye function, and

$$F_{\tau f} = \frac{2 - e^{-f\tau x} - e^{-f(1-\tau)x}}{x} \tag{9}$$

When $\tau = 0$ or 1, the graft copolymer degenerates to a linear diblock and $S(Q)$ clearly becomes Leibler's structure factor for linear diblocks. Since this is a mean-field theory, the position of the structure factor maximum Q^* is independent of temperature and the magnitudes of $S(Q^*)$ diverge at the spinodal temperature. Among the main predictions of the theory is that $S(Q)$ peaks at a higher Q, i.e., $Q^*_{\text{Graft}} > Q^*_{\text{Linear}}$, and that the phase diagram for a graft copolymer becomes asymmetric compared to a linear diblock, as a result of the inherent asymmetry of the former.

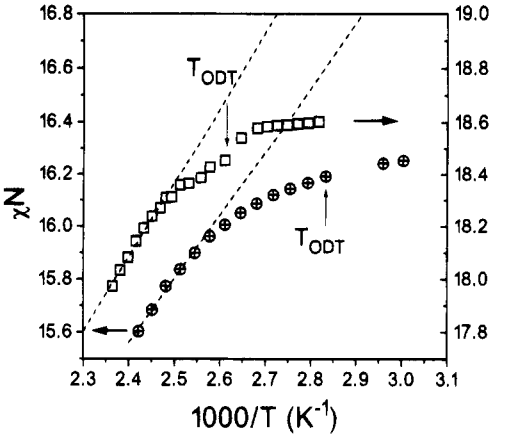

Figure 8. Temperature dependence of the interaction parameter for a linear SI diblock (⊕) and a simple graft SI2 copolymer (□) of the same composition ($f_{PS} \approx 0.27$).

It can be seen in Figure 7 that, although the intensity at Q^* increases sharply at the ODT, it stays at a finite value at temperatures below T_{ODT}. Furthermore, Q^* moves to higher values with increasing T, at $T \geq T_{ODT}$. Moreover, the theory fails in describing the experimental data as we approach the transition temperature. All these findings have been discussed for linear diblocks and prove that the MFT is not valid at least near the transition. At higher T, the agreement is good; however, χN and R_G are used as adjustable parameters and this agreement should not be taken as a proof for the accuracy of the MFT. An independent measurement of $R_G(T)$ and $\chi(T)$ can serve this purpose.

The temperature dependence of χN which is extracted from the fits to eqs 6−9 is plotted in Figure 8 for SI2 and compared with a linear diblock of the same composition ($f_{PS} = 0.27$). The χN values display a linear dependence when plotted versus inverse T only at high temperatures. Near the transition, χN becomes nearly independent of T. Notice the higher values for the graft copolymer as compared to the linear diblock which is in agreement with MFT. Notwithstanding the higher χN values in the former, the temperature dependence of χ extracted from high temperatures is $\chi_{\text{Linear}} = 0.037 + (9.2/T)$ and $\chi_{\text{Graft}} = 0.04 + (10/T)$. This means that, within the framework of the MFT, chain architecture may not be very important in determining the temperature dependence of the interaction parameter, at constant composition.

The inverse peak intensity, the peak width, and the peak position are plotted in Figure 9 vs inverse temperature. To have a consistent way of data evaluation below and above T_{ODT}, we have modeled the peak with a Lorentzian function, and these results are plotted in Figure 9. Evidently, at the ODT ($T_{ODT} = 379$ K) there are sharp discontinuities in all three parameters which amount to 45, 24, and 1.5% for the inverse peak intensity, peak width, and position, respectively. Notice the nonlinearity of $I(Q^*)^{-1}$ vs T^{-1} which is against the predictions of the MFT and which is reminiscent of linear diblocks near the ODT. The curvature of $I(Q^*)^{-1}$ vs T^{-1} and the absence of an intermediate bcc structure while heating through the ODT—both effects are known from linear diblocks—are manifestations of fluctuation effects. Computer simulations on graft copolymers[26] have also shown nonlinearities on $I(Q^*)^{-1}$ vs T^{-1} and provided evidence for non-Gaussian conformation near the transition.

Typical SAXS profiles for the 3-miktoarm star terpolymer SIB are also shown in Figure 7b for some

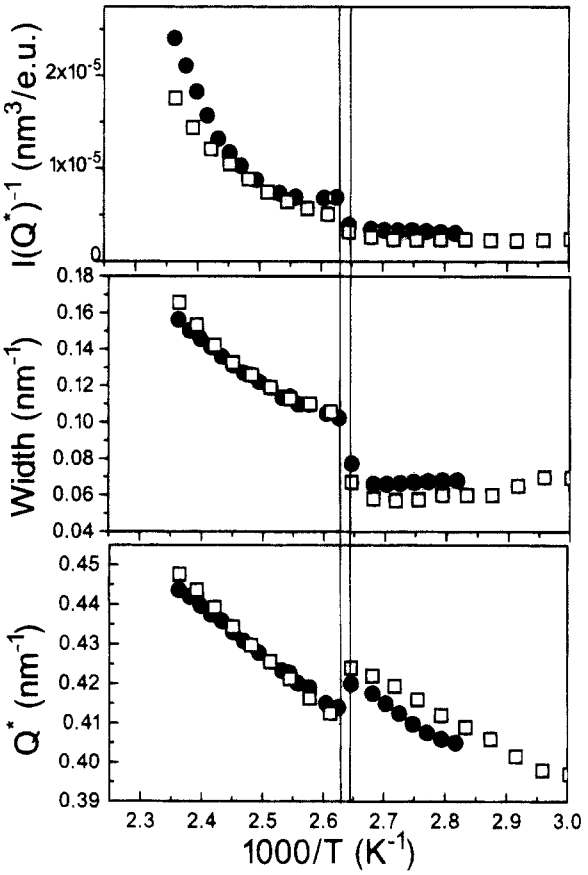

Figure 9. Inverse peak intensity, peak width, and peak position plotted vs inverse temperature for the graft SI2 (●) and the terpolymer SIB (□). The two vertical lines indicate the transition temperature.

temperatures. Similar to the graft copolymer SI2, there is a discontinuity in the peak intensity for temperatures between 383 and 373 K and this agrees with the estimation of T_{ODT} at 379 K on the basis of the two-dimensional SAXS patterns. The peak parameters for SIB are shown in Figure 9 and exhibit similar T dependence with the graft SI2. In order to extract an effective interaction parameter χ_{eff}, we have used an average segment volume and made the simplifying assumption that the miktoarm copolymer can be treated as a graft copolymer with $\tau = 0.5$. This assumption might sound like an oversimplification of the problem, but it is borne out by the same T_{ODT} for SI2 and SIB and most importantly from the very small interaction parameter between isoprene and butadiene, $\chi_{IB} = 4.68 \times 10^{-3} - (1.01/T)$, as compared to the interaction parameter between sytrene and butadiene, $\chi_{BS} = 8.4 \times 10^{-3} + (10.2/T)$, and between styrene and isoprene, $\chi_{SI}^{linear} = 0.037 + (9.2/T)$. χ_{IB} was determined from SANS[27] on blends of protonated polyisoprene with deuterated polybutadiene, whereas χ_{BS} was determined on the basis of the copolymer blend theory from the miscibility of binary blends of PB and poly(styrene-*b*-butadiene) (SBR).[28] At 379 K, χ_{BS} and χ_{SI} are respectively 18 and 30 times higher than χ_{BI}. The effective interaction parameter χ_{eff}^{SIB}, obtained from the fits to the MFT for a graft copolymer at high temperatures, gives $\chi_{eff} = 0.023 + (10.7/T)$. The parameters, $I(Q^*)^{-1}$, peak width, and peak position are discontinuous near the transition temperature as with the graft copolymer (Figure 9). In summary, the SAXS data for SI2 and SIB revealed that the isoprene and butadiene chains are mixed down to the molecular level. Additional support to this is

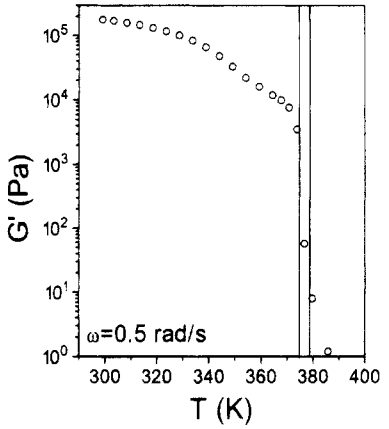

Figure 10. Temperature dependence of G' obtained at $\omega = 0.5$ rad/s and with low strain amplitude while heating the SIB terpolymer. The ODT is indicated with the two vertical lines ($T_{ODT} \approx 379$ K).

provided by the dynamics of the two systems and will be reported elsewhere.[29]

Rheology. The strain dependencies of G^*, shown in Figures 2 and 3 for SI2 and SIB, respectively, were used to locate the linear viscoelastic range. On the basis of this result, we have used strain amplitudes in the linear range and a low frequency ($\omega = 0.5$ rad/s) to perform the isochronal scans. The result for the temperature dependence of the storage modulus of SIB is shown in Figure 10. $G'(T)$, as obtained under heating, displays a discontinuity at a temperature ($T \approx 379$ K) which corresponds to the ODT. Thus, the T_{ODT} obtained from rheology is in excellent agreement with the one determined by SAXS, and the two methods provide unambiguous evidence for the structure formation. This point brings the question of whether the two methods probe structural changes at comparable length scales. Later we will attempt an answer to this problem with respect to the kinetic studies. Returning to Figure 10, we notice that the higher values of G' below 379 K correspond to the ordered states indicated by a sharp peak in the structure factor as probed by SAXS and at $T \geq 379$ K; the lower values of $G'(T)$ correspond to the lower values of $S(Q)$ above the T_{ODT} (Figure 9). An important observation in the T dependence of both G' and $S(Q)$ is that the distinction between the two levels in these quantities below and above ODT and the location of the discontinuities on the temperature scale are more precise when heating the sample. Under such thermal treatment, the kinetic effects—which we will study in detail in the next section—are largely decoupled from the temperature effects since the dissolution process studied in Figures 7, 9, and 10 occurs on a much faster time scale than the ordering process which is observed after quenching the sample from temperatures above the ODT. Therefore, isochronal scans at a (low) frequency which are performed under heating are most suitable for locating the T_{ODT} by rheology.

The localization of the T_{ODT} from rheology measured by isochronal scans is very precise, as presented in Figure 10; however, more information about the nature of changes in the sample related to the ODT can be obtained from a comparison of isothermal frequency sweeps performed below and above the ODT. The results of such experiments performed for SIB are shown in Figures 11 and 12. The frequency scans at various temperatures below and above the T_{ODT} have been recorded using as low strain amplitudes as possible. The principle of time–temperature superposition

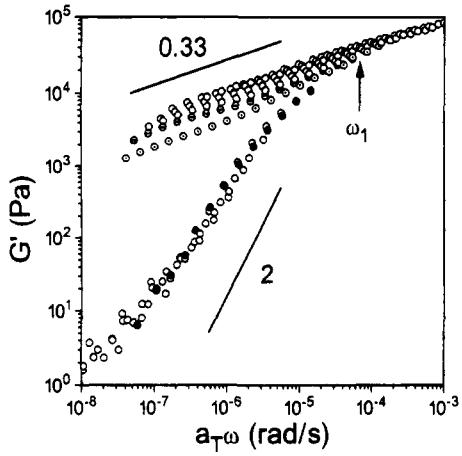

Figure 11. Reduced frequency plot for the G' data of SIB. Only data at some temperatures are marked: (⊖) 372, (⊙) 375, and (●) 383 K. Below the frequency ω_1, the shifted data split into two branches: one with a limiting slope of ~0.33 and another with 2 (terminal zone).

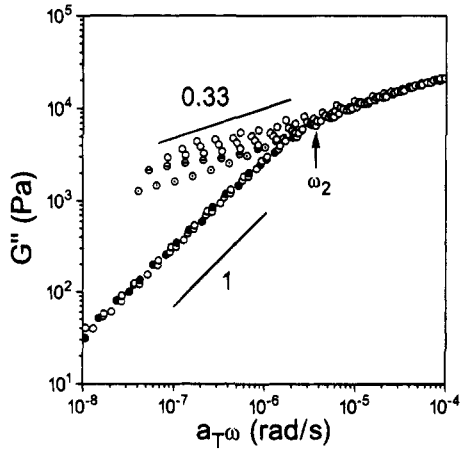

Figure 12. Reduced frequency plot for the G'' of SIB. The same shift factors as used in Figure 11 are used here. Only data at three temperatures are marked: (⊖) 372, (⊙) 375, and (●) 383 K. Below the frequency ω_2 there are again two branches with limiting slopes ~0.33 and 1 (terminal zone).

has been used by shifting the data along the logarithmic frequency scale with T_{ref} = 313 K. Block copolymers, in general, are not thermorheologically simple materials and this is also the case here; nevertheless, this method of data representation has shown to be a very useful tool for comparing results from different systems. The results of the attempted time–temperature superposition shown in Figures 11 and 12 indicate that for temperatures above T_{ODT} the master curves of G' and G'' have $G' \sim \omega^2$ and $G'' \sim \omega$ at low frequencies which is typical for the terminal zone of a polymer melt. Such behavior, characteristic of the Newtonian flow of the melt, suggests that the dynamics of the system above the T_{ODT} is controlled by a well-defined terminal relaxation time probably related to the relaxation of individual chains. The value of this terminal relaxation time which separates the terminal behavior of the system from the rubbery plateau can be estimated from the frequency at which G' and G'' cross each other. At temperatures below the T_{ODT} this behavior changes drastically. Only the high-frequency parts of G' and G'' frequency dependencies can be superimposed with the dependencies recorded above the T_{ODT}. At low frequencies, considerable deviations from the Newtonian flow are observed. Both dependencies of G' and G'' vs ω become almost parallel and assume the slope 0.33 which extends over some decades of frequency. Power law exponents of the same low value have also been reported for very asymmetric triblock copolymers.[30]

This kind of strongly non-Newtonian behavior with the parallel relationships of G' and G'' has been previously osberved for various other systems. Polystyrene μ-networks,[31a] comb-shaped polymers,[31b] and randomly branched polystyrenes,[31c] for networks where the cross-linking reaction was stopped upon gelation[31d] and for liquid crystalline states of poly(*p*-phenylene).[31e] In the case of the polystyrene μ-networks, this behavior has been attributed to the fractal nature of the system in that the network consists of a broad spectrum of relaxation times. In the case of the liquid crystalline systems, such behavior has been attributed to a distribution of domain sizes also leading to a broad distribution of their relaxation times. In the case of the block copolymers studied here, the interpretation might be similar as in the last case. The broad distribution of relaxation times being longer than the relaxation times of individual chains might be attributed to a broad distribution of sizes of grains with the microphase-separated morphology formed below the T_{ODT} via the nucleation and growth mechanism. This would imply that at the ODT the rheological behavior of the block copolymers changes from the Newtonian flow ($T > T_{ODT}$), controlled by the relaxation of individual chains, to the non-Newtonian behavior ($T < T_{ODT}$), controlled by relaxation of grains which rearrange with rates related to their sizes. The latter morphologically controlled mechanical behavior should be sensitive to the thermal and mechanical history of the sample as indeed experimentally observed.

The enlarged dynamic separation between the two branches in Figures 11 and 12 explains the large drop in $G'(T)$ (Figure 10) at ω = 0.5 rad/s. Furthermore, for the crossover frequency we have $\omega_1 \approx \tau^{-1}$, where τ is the characteristic longest relaxation time for individual coils, and this situation is different from linear entangled diblocks, where $\omega_1 \ll \tau^{-1}$. Only horizontal shifts were made for the G' (and G'') data shown in Figures 11 and 12, and the shift factors for SIB display the usual WLF behavior:

$$\log a_T = -\frac{C_1^0(T - T_0)}{C_2^0 + (T - T_0)} \qquad (10)$$

where C_1^0 and C_2^0 are the WLF parameters at the reference temperature T_0. These parameters assume the values 19.7 and 126, respectively, at 313 K. The shift factors for SI2 display a weak temperature dependence (Arrhenius), and this is probably the result of the smaller T range.

The result from an isochronal temperature scan, for a strain amplitude within the linear viscoelastic range (Figure 1), at ω = 0.5 rad/s while heating the graft copolymer SI2 is shown in Figure 13. The elastic modulus is discontinuous at T = 379 K which is in excellent agreement with the T_{ODT} obtained from SAXS. "Solid" and "liquid"-like behavior are separated by the two vertical lines in Figure 13. The drastic drop in $G'(T)$ at the ODT points to a large separation between the frequency dependence at low frequencies. This is shown in Figure 14, where data obtained isothermally are shifted horizontally using the principle of time–temperature superposition. Below a reduced frequency ω_1 there is again failure of the time–temperature superposition, and the data for the elastic modulus

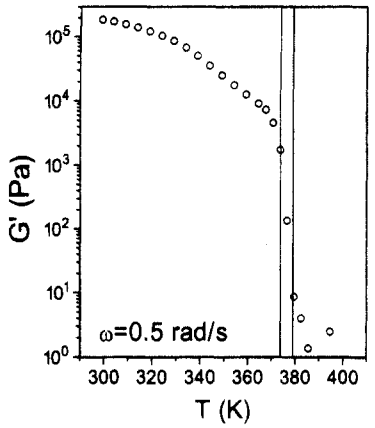

Figure 13. Temperature dependence of G' obtained at ω = 0.5 rad/s while heating the SI2 graft copolymer. The range of the ODT is indicated by the two vertical lines.

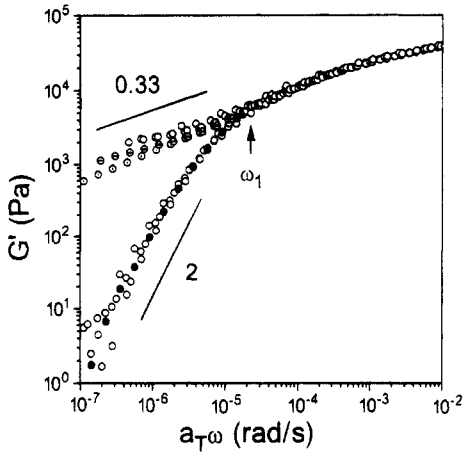

Figure 14. Reduced frequency plot for the G' data of SI2. Only data at three temperatures are marked: (⊖) 369, (⊙) 372, and (●) 381 K. The splitting frequency ω_1 is indicated, and the two branches with limiting slopes ~0.33 and 2 are also shown.

display two distinct frequency dependencies: one with a limiting slope of 2 and another with approximately 0.33. The former is characteristic of terminal-zone relaxation, whereas the latter is caused by the ordered structure below T_{ODT}. Moreover, $\omega_1 \approx \tau^{-1}_{SI2}$, as with the SIB star, and $\omega_1^{SI2} \approx \omega_1^{SIB}$ which implies that there is no dependence of ω_1 on the different architecture and that $\tau_{SIB} \approx \tau_{SI2}$, which is expected from the MW dependence of entangled melts ($\tau \sim N^{3.4}$) and the similar MW of the two copolymers (Table 1). An important observation on the rheology data of SI2 and SIB is that there is no evidence of fluctuations at $T > T_{ODT}$ when compared to the PEP–PEE system, which may be related to the smaller molecular weights used here. This situation contrasts the strong evidence of fluctuations from the SAXS data over the same temperature range. At $T < T_{ODT}$ the fluctuations can be studied by rheology and SAXS by probing the metastable states in the kinetic studies (below).

Ordering Kinetics. The ordering process in block copolymers bears some similarities with the crystallization process of semicrystalline materials. A variety of different experiments can be used to monitor the crystallization process, i.e., dilatometry,[32] X-ray diffraction,[33] rheology,[6,10] dielectric spectroscopy,[34] etc., but undoubtedly the most direct evidence is provided by dilatometry by recording the discontinuous change of the specific volume and of the isothermal compressibility as the material passes through the melting point. Our earlier work[24] on this subject has shown, however, that

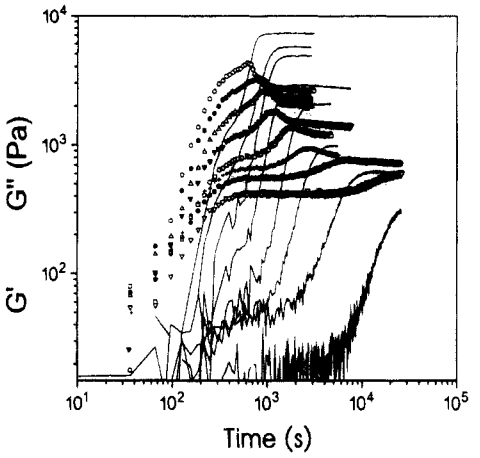

Figure 15. Time evolution of G' (lines) and G'' (symbols) for the SIB terpolymer following a quench from the disordered state (T_i = 385 K) to final temperatures (▽) 376.7, (⊖) 375.9, (+) 374.9, (□) 373.9, (▼) 371.7, (△) 369.6, (●) 367.6, and (○) 365.6 K. The frequency used was 0.5 rad/s, and the strain amplitude was 10% for the first three temperatures and less than 4% for the rest.

this method is not a sensitive probe of the ordering process in diblock copolymers, since both the density and the compressibility are continuous functions of T as a result of the weak first-order transition at the T_{ODT}. Herein we explored other indirect possibilities, namely, rheology and SAXS, with more emphasis on the former for reasons that will become clear below.

Knowledge of the T_{ODT} with a great accuracy is essential in studying the ordering kinetics in block copolymers. From SAXS and rheology we have established a T_{ODT} at 379 K for both copolymers. The first experiment is made by rheology using a small strain amplitude (below 10%) and involves isochronal/isothermal time scans at a frequency of 0.5 rad/s—which is well below the critical frequency—at selected temperatures. The specimen was heated in the rheometer at an initial temperature T_i = 385 K which is well above the ODT ($T_i = T_{ODT} + 6$ K). At this temperature, $G'(\sim\omega^2)$ and $G''(\sim\omega)$ display terminal behavior and are practically constant with time, since the sample is in the disordered state. Then, the temperature was dropped to the final temperature while shearing the sample, and the evolution of G' and G'' was studied for quenches to final temperatures 376.7, 375.9, 374.9, 373.9, 371.7, 369.6, 367.6, and 365.6 K for SIB and to temperatures 375.1, 374.6, 373.6, 372.6, 371.6, 369.6, 368.6, 365.6, 361.6, and 358.6 K for SI2. The evolutions of G' and G'' for SIB and SI2, following a quench from 385 K are shown in Figures 15 and 16, respectively. The storage moduli for both copolymers display a fast increase within the first 200–300 s and a second increase at longer times. The increase at short times is caused by the temperature drop to T_f and gives the lower limit to our resolution for the kinetic experiments.

The increase of G' at longer times occurs while the temperature has stabilized at T_f, and therefore this step is completely decoupled from temperature effects. Notice that while G' shows a sigmoidal shape at long times, the G'' data develop a maximum, especially for quenches away from T_{ODT}. This maximum is a consequence of the transition from a liquid-like behavior at short times (where the loss modulus exceeds the storage modulus) to a "solid-like" behavior at longer times (where the storage modulus exceeds the loss modulus). The plateau values of G' and G'' at short times are assumed to

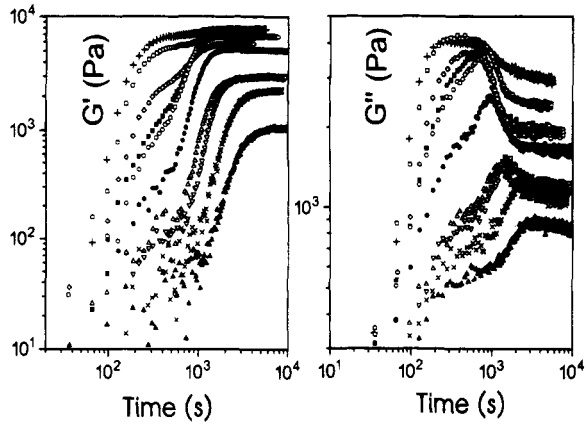

Figure 16. Time evolution of G' and G'' for the SI2 graft following a quench from the disordered state (T_i = 385 K) to final temperatures (▲) 375.1, (×) 374.6, (▽) 373.6, (△) 372.6, (●) 371.6, (○) 369.6, (■) 368.6, (◇) 365.6, (□) 361.6, and (+) 358.6 K. The frequency used was 0.5 rad/s, and the strain amplitude was 2%.

Scheme 1

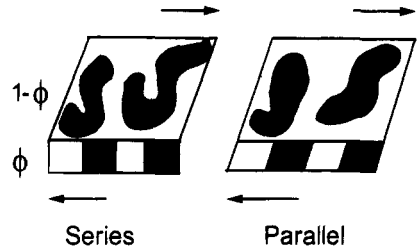

describe the viscoelastic properties of the disordered phase at the final temperature ($G' \sim \omega^2$, $G'' \sim \omega$). The plateau values at longer times are regarded as reflecting a mixed phase made out of the initial disordered and a newly developed ordered phase, the volume fraction of which increases with time.

The final plateau in Figures 15 and 16 is attained in a relatively short time with a shape which is reminiscent of the crystallization isotherms of semicrystalline materials. We will analyze subsequently the kinetics in terms of a nucleation and growth process of the Avrami type.[35] The aim is to extract the time-dependent volume fraction of the ordered phase $\phi(t)$, and for this purpose we will use the two simplest "series" and "parallel" mechanical models. The two models are shown in Scheme 1. In the series model, the same stress is applied to both phases (ordered and disordered), and this results in different displacements. The modulus of the mixed phase is expressed as a linear combination of the compliances of the constituent phases:

$$\frac{1}{G(t)} = \frac{1-\phi(t)}{G_0} + \frac{\phi(t)}{G_\infty} \tag{11}$$

where $G(t)$ $(=(G'^2(t) + G''^2(t))^{1/2})$ is the absolute value of the complex modulus and G_0 and G_∞ are the moduli of the initial ($t = 0$) disordered and final ($t = \infty$) ordered phases, respectively. In the "parallel" model the two phases have the same displacement but different stresses and the modulus of the mixed phase can be expressed as a linear combination of the moduli of the constituent

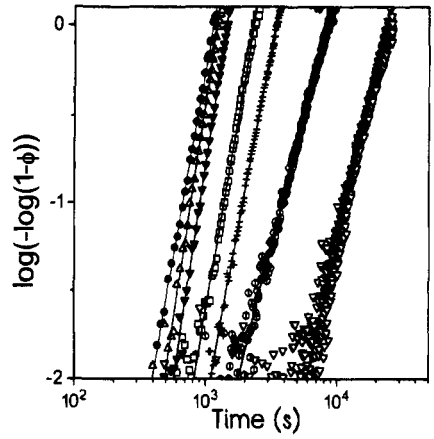

Figure 17. Avrami plots for the volume fraction of the ordered phase $\phi(t)$ of SIB. The symbols are the same as in Figure 15. Solid lines are fits to the Avrami equation (eq 13).

phases:

$$G(t) = (1 - \phi(t))G_0 + \phi(t)\, G_\infty \tag{12}$$

In the case of linear diblocks we were able to extract $\phi(t)$ from both moduli (eqs 11 and 12) and the differences between the two were found to be small. In the present case, where $G''(t)$ develops a maximum, we can only use the series model to calculate $\phi(t)$ from $G(t)$ and the limiting values of G_0 and G_∞. The time dependence of ϕ obtained from the series model at every temperature is analyzed by fitting the Avrami equation:

$$\phi(t) = 1 - \exp(-\alpha t^n) \tag{13}$$

where α is the rate constant and n is the Avrami exponent. The former gives quantitative information on the course of "crystallization" and it is usually expressed in terms of the half-time (or completion time):

$$t_{1/2} = (\ln 2/\alpha)^{1/n} \tag{14}$$

The Avrami exponent n is a combined function of the growth dimensionality and of the time dependence of the nucleation process and provides qualitative information on the nature of the nucleation and growth process. The Avrami parameters are usually extracted from a plot of $\log(-\log(1 - \phi))$ vs $\log t$ from which it is possible to derive n and α from the slope and intercept, respectively. This way of plotting the SIB data is shown in Figure 17. The evolution of the volume fraction of the ordered phase can be described by the Avrami equation for the major part of the crystallization process; only at longer times do some deviations occur. There are two pertinent features in Figure 17. First, there is a pronounced temperature effect on the kinetics. Quenching the sample to final temperatures near the ODT makes the kinetics very slow with times which depend strongly on the final temperature but quenching to temperatures further below (i.e., to T_f = 369.6 and 367.7 K) produces only moderate changes on the kinetics. Second, there is a change in slope in going from low to high undercooling.

Similar results have been obtained for the SI2 graft copolymer, and the Avrami parameters are plotted in Figure 18 and compared with a linear diblock at temperatures equidistant from the T_{ODT}. For shallow quenches ($T_{ODT}-T$ = 3 K) the kinetic times $t_{1/2}$ change considerably but are nearly indistinguishable for a 3-miktoarm star terpolymer (SIB), a graft copolymer

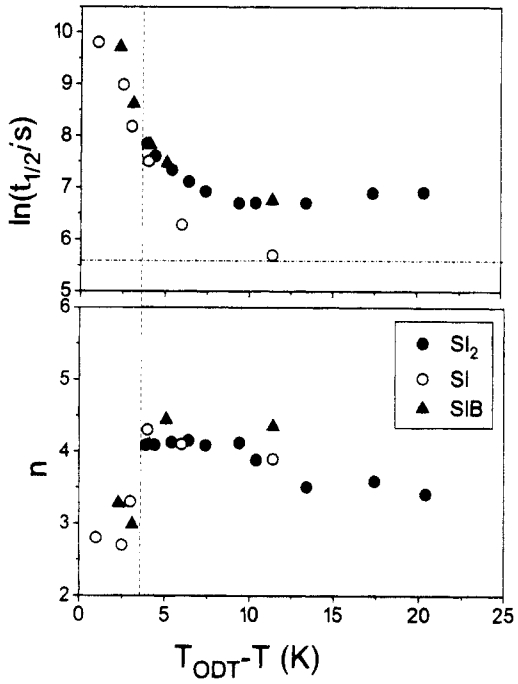

Figure 18. Parameters of the Avrami equation: ln $t_{1/2}$ and exponent n plotted for a linear diblock (SI), a simple graft copolymer (SI2), and a 3-miktoarm star terpolymer (SIB) as a function of $T_{ODT}-T$. The horizontal line in the upper plot is the limiting time due to the experimental resolution. The vertical line separates two regimes (see text).

(SI2), and a linear diblock (SI).[10] For deeper quenches there is a clear difference in $t_{1/2}$ between the linear and graft copolymers. The width of the kinetically accessible metastable region is larger for the graft copolymer and miktoarm star terpolymer as compared to the linear diblock, with no apparent relation to the T_g of the styrene-rich phase since $\Delta(T_{ODT}-T_g^S) \approx 25$, 41, and 44 K for SI, SIB, and SI2, respectively. The reason for the different metastability gap may be associated with the different morphology (cylinders vs lamellae) of the 3-miktoarm star polymers and linear copolymers.[36] Furthermore, the Avrami exponent n changes from a value of about 3 for shallow quenches to about 4 for deeper quenches, reflecting a change in the mechanism of structure formation. Since the Avrami exponent is a combined function of the growth dimensionality and of the time dependence of the ordering process, a definite conclusion on the type of crystallization (homogeneous vs heterogeneous) cannot be made based only on the values of n shown in Figure 18. A clue for the type of crystallization can be obtained by plotting the characteristic time $t_{1/2}$ vs δ^{-1} (heterogeneous) or δ^{-2} (homogeneous nucleation), where δ is a dimensionless undercooling parameter defined as $\delta = (\chi - \chi_{ODT}/\chi_{ODT}) > 0$, where χ_{ODT} and χ are values of the interaction parameter at the ODT and at the final temperatures. Before we realize this comparison for the SI2 graft copolymer in Figure 19, we need to make a comment on the way the χ parameter is obtained at temperatures *below* the T_{ODT}. The linear relation between χ and T^{-1} is used from the high temperatures (Figure 8) and an extrapolation is made to temperatures $T \leq T_{ODT}$, and the result is shown in Figure 19. Excluding data points for the deep quenches where the kinetic times are nearly independent of T, we find that the ln $t_{1/2}$ can be better linearized when plotted vs δ^{-1}, and this is also the case with the 3-miktoarm star terpolymer SIB and the linear SI. This brings forward the picture of heterogeneous

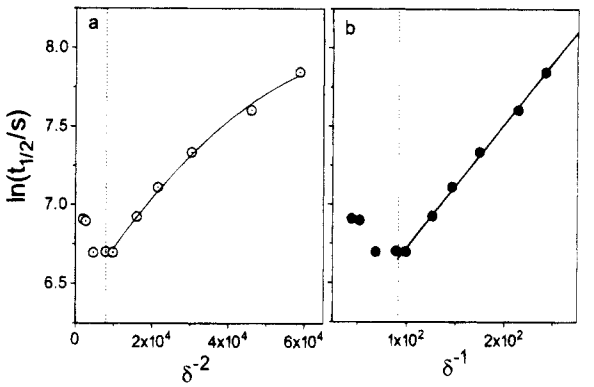

Figure 19. Characteristic time $t_{1/2}$ plotted vs the undercooling parameter δ for two cases: (a) homogeneous and (b) heterogeneous nucleation.

nucleation. Based on the notion for the heterogeneous type of nucleation, the Avrami exponent of $n = 3$ for shallow quenches indicates that the ordering proceed by heterogeneous nucleation and growth of three-dimensional grains with lamellar (SI diblock) or cylindrical (3-miktoarm star polymers) microstructure. For deeper quenches, the kinetic curves change in shape ($n \approx 4$), indicating a different mechanism of structure formation. The unreasonably high Avrami exponent for a heterogeneous nucleation could imply that for deep quenches the ordering proceeds by spinodal decomposition (SD) rather than by nucleation and growth.

The nucleation barriers for the order–disorder transition have been calculated for a symmetric[37] diblock and generalized for asymmetric[38] linear diblocks. The theory is based on the fluctuation picture and assumes homogeneous nucleation. The nucleation barrier in the case of symmetric diblocks is given by:

$$\frac{\Delta F^*}{k_B T} \sim \bar{N}^{-1/3}\delta^{-2} \tag{15}$$

with the familiar $\bar{N}^{-1/3}$ fluctuation term, whereas for asymmetric diblocks it is anomalously large:

$$\frac{\Delta F^*}{k_B T} \sim \bar{N}^{1/2}|f - 0.5|^5\delta^{-2} \tag{16}$$

Earlier work on the symmetric diblock copolymers PEP–PEE[6] and SI[10] have shown that the theory can only qualitatively describe the experimental results but fails to account for the kinetics in a more quantitative manner. The reasons for the deviations are related to the slight asymmetry of the samples, the polydispersity, and the fact that in all systems the ordering proceeds by heterogeneous nucleation. For the 3-miktoarm star (graft) copolymer and terpolymer investigated here there is, to our knowledge, no theoretical work on the ordering kinetics.

In a separate rheological experiment we have investigated the effect of shear on the ordering kinetics. That is, we studied whether shearing a specimen *while* quenching it to T_f has any effect in inducing, accelerating, or impeding the ordering process. The experiment was made with the SIB terpolymer for a quench to $T_f = 365.7$ K from $T_i = 388$ K at a frequency of 0.5 rad/s and a strain amplitude of 2%. The experiment consisted of four steps: in the first step, oscillatory shear was applied while quenching the sample to T_f. The result is shown with a solid line in Figure 20. In the next step, the sample is heated again to T_i and quenched to T_f

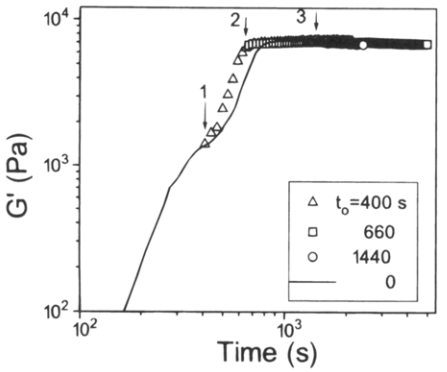

Figure 20. Time evolution of G' for the terpolymer SIB, obtained after quenching from the disordered state (T_i = 385 K) to T_f = 365.7 K under continuous oscillatory shear (solid line). Different symbols correspond to different quenches to the same final temperature, and arrows indicate the delay time t_0, after which oscillatory shear has been applied.

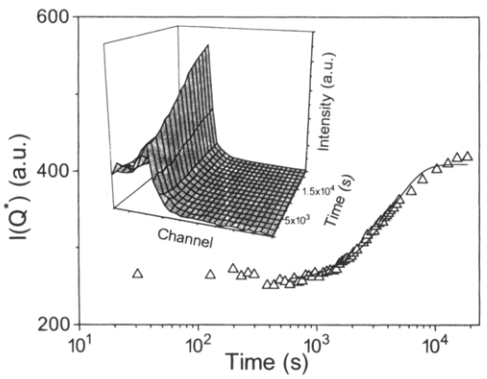

Figure 21. Evolution of the scattered intensity at Q^* following a jump from T_i = 403 K to a final temperature T_f = 365.6 K which is below the T_{ODT} (≈379 K) of the SI2 graft copolymer. The SAXS profile is shown in the inset as a function of time.

without shearing the sample for t_0 = 400 s. After this time oscillatory shear is applied. For the other two steps a delay time of 660 and 1440 s was used. The offset of the data points in Figure 20 from the solid line is caused by a small difference in the T_f in the first step. Evidently, application of continuous oscillatory shear—within the linear viscolelastic range—while cooling a copolymer through the ODT does *not* affect the ordering kinetics. The ordering proceeds with the same characteristic time ($t_{1/2}$) and shape (n) independent from the external perturbation.

The ordering kinetics have also been studied by SAXS. The SI2 sample was heated to T_i = 403 K and held there for about 20 min in a furnace outside the camera. The camera was set to different final temperatures: T_f = 374.9, 372.6, 369.6, 365.6, 361.6, and 358.6 K below the T_{ODT} (=379 K). Then, the sample was quickly transferred to the camera, and the temperature in the sample was continuously monitored. With this procedure it took about 100 s for the sample to reach thermal equilibrium at T_f. The intensity profile was subsequently monitored in intervals of 10−60 s. Figure 21 shows the gradual increase in the peak intensity as a function of time for a quench to T_f = 365.6 K. The scattering intensity (inset to Figure 21) changes from a rather broad liquid-like peak to a narrow solid-like peak, and this change is completed within ~2 × 10^4 s. The peak intensity $I(Q^*,t)$ changes by a factor of 2 in going from the disordered to the ordered state (see also Figure 7), and the shape of $I(Q^*,t)$ can be fitted to the Avrami equation with an exponent of $n \approx 2$. A fair comparison between the rheological and SAXS kinetic studies requires the extraction of the same quantity, namely, the volume fraction of the ordered phase. In SAXS, this quantity can be extracted by measuring the total scattering power of the medium:

$$P = \frac{1}{2\pi^2}\int_0^\infty Q^2 I(Q)\, dQ \tag{17}$$

which is evaluated from the scattering intensity integrated over all Q. For an ideal two-phase system, the scattering power depends on the relative amounts of the volume fraction of the ordered (ϕ) and disordered ($1 - \phi$) phases:

$$P \sim \Delta n^2 \phi(1 - \phi) \tag{18}$$

where Δn is again the electron density difference between the two phases. $P(t)$ evaluated from eq 17 has a time dependence similar to that of $I(Q^*,t)$ and can be fitted with an Avrami exponent of $n \approx 2$. Similar (low) Avrami exponents have been reported in other kinetic studies by SAXS.[5,9,33] This value is smaller than the one obtained from rheology for a quench to the same final temperature, but the origin of this difference is not yet clear to us. A certain advantage in using rheology for the kinetic studies is that, by choosing a convenient (low) frequency, one can make the step in $G^*(t)$ become large (usually 1 order of magnitude), whereas the observed change in $I(Q^*,t)$ can be a factor of 2 at most.

Conclusion

The results from the first SAXS and rheological study on the statics and kinetics of a simple graft and a 3-miktoarm star terpolymer can be summarized as follows. With respect to the statics: the SAXS data revealed sharp discontinuities in all profile parameters at temperatures near the ODT. At high enough temperatures ($T \gg T_{ODT}$) the MFT for graft copolymers describes the scattering profiles quantitatively. However, near the ODT, it fails to fit the experimental data and the peak position, Q^*, shifts to higher values. This fact, together with the pronounced curvature in the plot of $I(Q^*)^{-1}$ vs T^{-1} and the absence of an intermediate bcc structure, is a manifestation of the fluctuation effects which become important near the transition. The rheological study gave also evidence for a sharp discontinuity in $G'(T)$ at the ODT, and the transition temperature from rheology was found to be in excellent agreement with the one from SAXS.

With respect to the kinetic studies we found that the ordering kinetics in linear, simple graft copolymers and 3-miktoarm star terpolymers are reminiscent of the crystallization isotherms of semicrystalline materials (of the Avrami type). The width of the kinetically accessible metastable region is larger for the graft copolymer and the star terpolymer as compared to the linear diblock with no apparent relation to the polystyrene glass transition. For shallow quenches ($T_{ODT} - T \approx 3$ K) ordering proceeds by heterogeneous nucleation and growth of three-dimensional grains with lamellar (symmetric diblocks) or cylindrical (3-miktoarm star polymers) microstructure. For deeper quenches, the kinetic curves change in form, indicating a different mechanism of structure formation. Our rheological and SAXS kinetic studies directly probe the metastable states near the ODT which are manifestations of fluctuation effects.

Note Added in Proof: Fluctuation corrections to the mean-field phase diagram for graft copolymers (I. Ya. Erukhimovich, private communication) confirm the absence of the intermediate bcc structure (Figure 6). A quantitative comparison with the corrected phase diagram is in progress.

References and Notes

(1) See, for example: Bates, F. S.; Fredrickson, G. H. *Annu. Rev. Phys. Chem.* **1990**, *41*, 525.
(2) Leibler, L. *Macromolecules* **1980**, *13*, 1602.
(3) Fredrickson, G. H.; Helfand, E. *J. Chem. Phys.* **1987**, *87*, 697.
(4) Bates, F. S. *Macromolecules* **1984**, *17*, 2607.
(5) Bates, F. S.; Rosedale, J. H.; Fredrickson, G. H. *J. Chem. Phys.* **1990**, *92*, 6255.
(6) Rosedale, J. H.; Bates, F. S. *Macromolecules* **1990**, *23*, 2329.
(7) Gehlsen, M. D.; Almdal, K.; Bates, F. S. *Macromolecules* **1992**, *25*, 939.
(8) Stühn, B.; Mutter, R.; Albrecht, T. *Europhys. Lett.* **1992**, *18*, 427.
(9) Schuler, M.; Stühn, B. *Macromolecules* **1993**, *26*, 112.
(10) Floudas, G.; Pakula, T.; Fischer, E. W.; Hadjichristidis, N.; Pispas, S. *Acta Polym.* **1994**, *45*, 176.
(11) Mayes, A. M.; Olvera de la Cruz, M. *J. Chem. Phys.* **1989**, *91*, 7828.
(12) Olvera de la Cruz, M.; Sanchez, I. C. *Macromolecules* **1986**, *19*, 2501.
(13) Benoit, H.; Hadziioannou, G. *Macromolecules* **1988**, *21*, 1449.
(14) Shinozaki, A.; Jasnow, G.; Balazs, A. C. *Macromolecules* **1994**, *27*, 2496.
(15) Mayes, A. M.; Olvera de la Cruz, M. *J. Chem. Phys.* **1991**, *95*, 4670.
(16) Dobrynin, A. V.; Erukhimovich, I. Ya. *J. Phys. II(Fr.)* **1991**, *1*, 1387. Dobrynin, A. V.; Erukhimovich, I. Ya. *Macromolecules* **1993**, *26*, 276.
(17) Iatrou, H.; Hadjichristidis, N. *Macromolecules* **1992**, *25*, 4649.
(18) Hadjichristidis, N.; Iatrou, H.; Behal, S. K.; Chludzinski, J. J.; Disko, M. M.; Garner, R. T.; Liang, K. S.; Lohse, D. J.; Milner, S. T. *Macromolecules* **1993**, *26*, 5812.
(19) Iatrou, H.; Hadjichristidis, N., to be published.
(20) Morton, M.; Fetters, L. *J. Rubber Chem. Technol.* **1975**, *48*, 359.
(21) Winter, H. H.; Scott, B. D.; Gronski, W.; Okamoto, S.; Hashimoto, T. *Macromolecules* **1993**, *26*, 7236.
(22) For symmetric diblocks two distinct lamellae orientations ("perpendicular" and "parallel") have been observed: Koppi, K. A.; Tirrell, M.; Bates, F. S.; Almdal, K.; Colby, R. H. *J. Phys. II* **1992**, *2*, 1941.
(23) Almdal, K.; Bates, F. S.; Mortensen, K. *J. Chem. Phys.* **1992**, *96*, 9122.
(24) Floudas, G.; Vogt, S.; Pakula, T.; Fischer, E. W. *Macromolecules* **1993**, *26*, 7210.
(25) Floudas, G.; Pakula, T.; Fischer, E. W. *Macromolecules* **1994**, *27*, 917.
(26) Gauger, A.; Pakula, T. *Macromolecules*, in press.
(27) Hasegawa, H.; Sakurai, S.; Takenaka, M.; Hashimoto, T.; Han, C. C. *Macromolecules* **1991**, *24*, 1813.
(28) Sakurai, S.; Izumitani, T.; Hasegawa, H.; Hashimoto, T.; Han, C. C. *Macromolecules* **1991**, *24*, 4844.
(29) Floudas, G.; Fytas, G.; Iatrou, H.; Hadjichristidis, N., in preparation.
(30) Adams, J. L.; Graessley, W. W.; Register, R. A. *Macromolecules*, preprint.
(31) (a) Antonietti, M.; Foelsch, K. J.; Sillescu, H.; Pakula, T. *Macromolecules* **1989**, *22*, 2812. (b) Roovers, J.; Graessley, W. W. *Macromolecules* **1981**, *14*, 766. (c) Masuda, T.; Ohta, Y.; Onogi, S. *Macromolecules* **1986**, *19*, 2524. (d) Winter, H. H.; Chambon, F. *J. Rheol.* **1986**, *30* (2), 367. (e) McCarthy, T. F.; Pakula, T.; Wegner, G., to be published.
(32) Fakhredline, Y. A.; Zoller, P. *J. Polym. Sci., Polym. Phys. Ed.* **1991**, *29*, 1141.
(33) Stühn, B.; Vilesov, A.; Zachmann, H. G. *Macromolecules* **1994**, *27*, 3560.
(34) Coburn, J. C.; Boyd, R. H. *Macromolecules* **1986**, *19*, 2238.
(35) Avrami, M. J. *J. Chem. Phys.* **1939**, *7*, 1103; **1940**, *8*, 212; **1941**, *9*, 177.
(36) A similar temperature dependence of the kinetic times has been reported for polyurethanes. Koberstein, J., private communication.
(37) Fredrickson, G. H.; Binder, K. *J. Chem. Phys.* **1989**, *91*, 7265.
(38) Binder, K. *Physica A*, preprint.